


Metallic quantized anomalous Hall effect without chiral edge statesKai-Zhi Bai¹, Bo Fu², Zhenyu Zhang³ and Shun-Qing Shen^{1,4,*}¹*Department of Physics, The University of Hong Kong, Pokfulam Road, Hong Kong, China*²*School of Sciences, Great Bay University, Dongguan, China*³*Hefei National Laboratory of Physical Sciences at the Microscale, University of Science and Technology of China, Hefei, Anhui 230026, China*⁴*Quantum Science Center of Guangdong-Hong Kong-Macau Greater Bay Area, China* (Received 11 August 2023; revised 27 October 2023; accepted 12 December 2023; published 28 December 2023)

The quantum anomalous Hall effect (QAHE) is a topological state of matter with a quantized Hall resistance. It has been observed in some two-dimensional insulating materials such as magnetic topological insulator films and twisted bilayer graphene. These materials are insulating in the bulk but possess chiral edge states carrying the edge current around the system. Here we discover a metallic QAHE in a topological insulator film with a magnetic sandwich heterostructure, in which the Hall conductance is quantized to e^2/h but the longitudinal conductance remains finite. This effect is attributed to the existence of a pair of massless Dirac cones of surface fermions, with each contributing half of the Hall conductance due to the quantum anomaly. It is not characterized by a Chern number and is not associated with any chiral edge states. Our study offers insights into topological transport phenomena and topological metallic states of matter.

DOI: [10.1103/PhysRevB.108.L241407](https://doi.org/10.1103/PhysRevB.108.L241407)

Introduction. The quantum anomalous Hall effect (QAHE) is a quantum transport phenomenon in two-dimensional ferromagnetic materials in which the Hall resistance is quantized to the von Klitzing constant h/e^2 while the longitudinal resistance disappears [1–7]. The materials are band insulators in the bulk and possess chiral edge states carrying a dissipationless electric current around the system boundary [8,9]. The electronic band structures of the materials are characterized by the Chern number [10,11], which equals the number of chiral edge states [12]. Over the last decade the effect has been observed experimentally in a series of topological insulator (TI) films and two-dimensional materials [13–24]. The picture of the chiral edge states is also confirmed experimentally [25,26]. Recently, the half-quantized Hall conductance was reported in a magnetic doped TI film [27]. The power-law decay of the Hall current indicates the possible existence of a distinct QAHE which is not characterized by the Chern number or chiral edge state [28,29]. This provides a possible route to explore novel types of QAHE.

A TI film hosts a pair of massless Dirac cones of electrons near the two surfaces. The exchange interaction of magnetic ions or ferromagnetic magnetization breaks time-reversal symmetry and may manipulate the nature of the surface states [30]. Here we propose a unique type of QAHE with no chiral edge states in a magnetically doped TI film in which the Hall conductance is quantized to be e^2/h while the longitudinal conductance is finite. The Hall resistivity is then not quantized. The magnetically doped layers are confined near the center to form a sandwich structure, as illustrated in Fig. 1. Based on numerical calculation and analytical analysis of the film, it is observed that increasing the concentration

x of doped Cr atoms or increasing the Zeeman field may induce a transition of the Hall conductance from zero to $-e^2/h$; meanwhile, the band structure shows that no energy gap opens as the magnetically doped layer is far away from the top and bottom surfaces. Further analysis shows that the TI film hosts a pair of massless Dirac fermions; one carries $e^2/2h$, and the other carries $-e^2/2h$ of the Hall conductance in the absence of the Zeeman field. An increasing Zeeman field drives one of the gapless Dirac cones and the accompanying gapped Dirac cone to exchange their masses, and the sign of the Hall conductance changes from $e^2/2h$ to $-e^2/2h$. Consequently, the total Hall conductance becomes $-e^2/h$ (the sign is determined by the direction of the Zeeman field). The longitudinal conductance is finite, as no gap opens in the surface states, and has a minimal value when the chemical potential sweeps the Dirac point of the surface electrons. Hence, chiral edge states localized near the system boundary do not exist.

Magnetic sandwich TI film. We consider a symmetric TI film with a magnetic doped layer at the center $m\text{QLX}_2\text{Te}_3/3\text{QLX}_{2-x}\text{Cr}_x\text{Te}_3/m\text{QLX}_2\text{Te}_3$, with $X = \text{Bi}, \text{Sb}$ and $m = 4$, as shown in Fig. 1. A larger integer m does not change the main result in this proposal. Bi_2Te_3 and Sb_2Te_3 are prototypes of strong TIs [31]. Here 1QL indicates a quintuple layer of X and Te atoms and is about 1 nm in Bi_2Te_3 . The Dirac cone of surface states was observed explicitly using angle-resolved photoemission spectroscopy [32,33] and was also evidenced by a series of transport measurements. The exchange interaction between the p -orbital electron from Bi and Te and magnetic ions of Cr may induce a finite magnetization in $X_{2-x}\text{Cr}_x\text{Te}_3$ [2,30]. Tuning the concentration x of Cr can change the exchange interaction and even makes it a ferromagnetic insulator [34]. The magnetic element Cr was modulation doped only near the center layer. The nondoped layers are thick enough that the top and bottom surface elec-

*sshenn@hku.hk

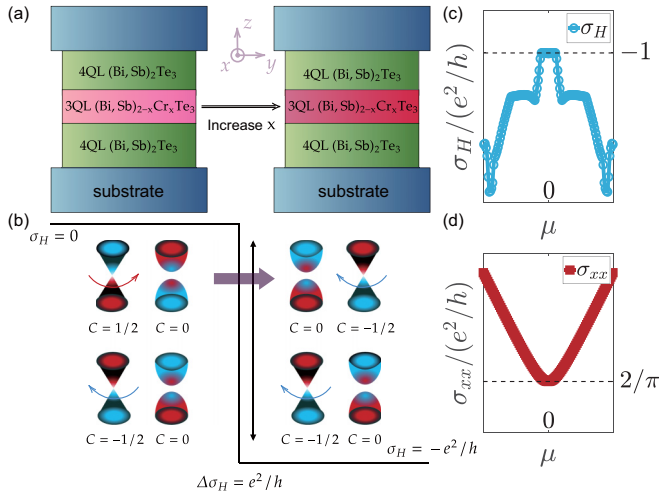


FIG. 1. (a) Schematic of the magnetic sandwich heterostructure of a $(\text{Bi, Sb})_2\text{Te}_3$ TI film with the concentration x of magnetically doped Cr atoms. (b) The transition from two pairs of massless and massive Dirac fermions with no net Hall conductance $\sigma_H = 0$ at low concentration x to those with a quantized Hall conductance $\sigma_H = -\frac{e^2}{h}$ at higher concentration x (the sign depends on the direction of magnetization). C represents the Hall conductance in units of e^2/h , while the color represents the sign value of the Berry curvature, with blue for negative and red for positive. The masses of a pair of massless and massive Dirac fermions (in the horizontal row) at lower energy are exchanged by increasing the concentration x , while the higher-energy parts of the Dirac fermions remain almost unchanged. (c) Schematic of the quantized Hall conductance σ_{xy} and (d) the longitudinal conductivity σ_{xx} as a function of the chemical potential μ at a higher doping concentration x .

trons do not open an energy gap. The topological nature of the band structures of Bi_2Se_3 and Bi_2Te_3 can be well described by the tight-binding model for the electrons of the $P_{z,\uparrow}$ and $P_{z,\downarrow}$ orbitals from Bi and Te or Se atoms near the Fermi energy [31,35],

$$H_{\text{TI}} = \sum_l \Psi_l^\dagger \mathcal{M} \Psi_l + \sum_{l,\alpha=x,y,z} (\Psi_l^\dagger \mathcal{T}_\alpha \Psi_{l+\alpha} + \Psi_{l+\alpha}^\dagger \mathcal{T}_\alpha^\dagger \Psi_l), \quad (1)$$

where $\mathcal{M} = (m_0 - 2 \sum_\alpha t_\alpha) \sigma_0 \tau_z$, $\mathcal{T}_\alpha = t_\alpha \sigma_0 \tau_z - i \frac{\lambda_\alpha}{2} \sigma_\alpha \tau_x$, and Ψ_l^\dagger and Ψ_l are the four-component creation and annihilation operators at position $l = (l_x, l_y, l_z)$. The Pauli matrices σ_α and τ_α act on the spin and orbital indices, respectively. Adapting a model homogeneous in the $x - y$ plane leads to $t_{\parallel} = t_x = t_y$, $t_{\perp} = t_z$, $\lambda_{\parallel} = \lambda_x = \lambda_y$, and $\lambda_{\perp} = \lambda_z$. The magnetic effect induced by Cr is modeled by introducing the Zeeman field along the z direction, $V_z = \sum_l V_z(l_z) \Psi_l^\dagger \sigma_z \tau_0 \Psi_l$. $V_z(l_z) = \alpha t_{\perp}$ in the magnetic doped layers (using t_{\perp} as a unit), with $l_z = \pm 1/2, \dots, \pm(m_z - 1)/2$, where film thickness L_z and the magnetic layer thickness m_z are assumed to be even, and equals zero in the nondoped layers. Here we ignore the possible change in the bulk gap m_0 in $X_{2-x}\text{Cr}_x\text{Te}_3$ caused by doping.

We consider the periodic boundary condition in the x and y directions. The band structure of the film is calculated numerically by means of the exact diagonalization method as

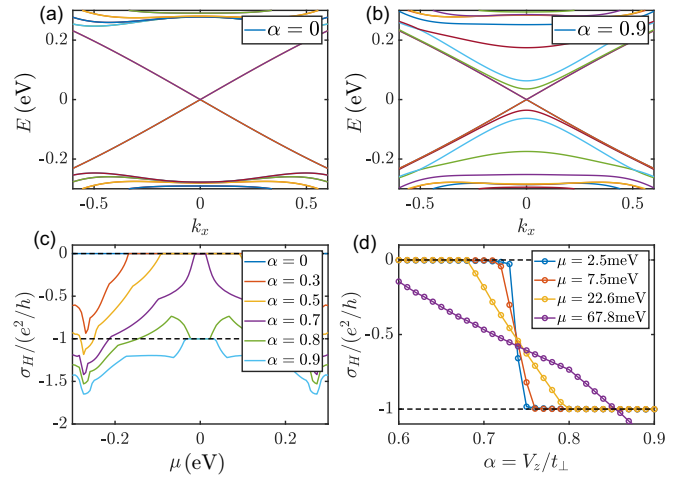


FIG. 2. The band structure near the Γ point with $k_y = 0$ (a) in the absence of magnetic doping ($\alpha = 0$) and (b) in the presence of magnetic doping ($\alpha = 0.9$). The gapless dispersions for the surface states in (a) and (b) are doubly degenerate. (c) The calculated Hall conductance as a function of the chemical potential μ . (d) The Hall conductance as a function of α at different chemical potentials. We set the model parameters as $\lambda_{\parallel} = 0.41$ eV, $\lambda_{\perp} = 0.44$ eV, $t_{\parallel} = 0.566$ eV, $t_{\perp} = 0.4$ eV, $m_0 = 0.28$ eV, $a = b = 1$ nm, and $c = 0.5$ nm if there is no other specific indication [31]. The thickness $L_z = 22$, and the magnetic layers $m_z = 6$. One QL is about $2c = 1$ nm.

shown in Fig. 2(a) in the absence of magnetic layers ($\alpha = 0$) and Fig. 2(b) in the presence of magnetic layers ($\alpha = 0.9$). It is observed that a pair of massless Dirac fermions exists in both cases. The dispersions are doubly degenerate near the crossing point at $k = 0$. The presence of the Zeeman field α does not open an energy gap in the surface states while α varies from 0 to 0.9. It is reasonable that the massless surface electrons are mainly located near the top and bottom surfaces, which are far away from the magnetic ions in the magnetic layers (see Fig. S3 in the Supplemental Material [36]). With the numerical energy eigenvalues and eigenvectors, the Hall conductance can be calculated numerically by means of the Kubo formula for electric conductivity [37]. The Hall conductance becomes nonzero in the presence of α when the Fermi level crosses the conduction and valence bands with $n > 1$. As shown in Fig. 2(c), a plateau of zero Hall conductance appears near $\mu = 0$ for a weak field, while for a strong Zeeman field α , a flat plateau of $\sigma_H = -\frac{e^2}{h}$ appears. The detailed calculation presented in Fig. 2(d) shows the Hall conductance changes from zero to $-\frac{e^2}{h}$ with increasing Zeeman field α for fixed chemical potentials. Considering that there is no band gap while α changes from 0 to 0.9, the longitudinal conductivity must be finite. Thus, the appearance of the Hall conductance indicates that it differs from the conventional QAHE in an insulating phase.

Equivalent Dirac-like fermions. To explore the physical origin of the quantized Hall conductance, we study the band structure of the film in the presence of the Zeeman field. First, we adopt the Fourier transformation $\Psi_{l_z, \mathbf{k}} = \sum_{l_x, l_y} \exp[i l_x k_x + i l_y k_y] \Psi_{l_x, l_y, l_z}$. The tight-binding model in Eq. (1) with the Zeeman field $H_{\text{tot}} = H_{\text{TI}} + V_z$ can be split into two parts, $H_{\text{tot}} = H_{\parallel} + H_{\text{1D}}(\alpha)$. The in-plane spin-orbital

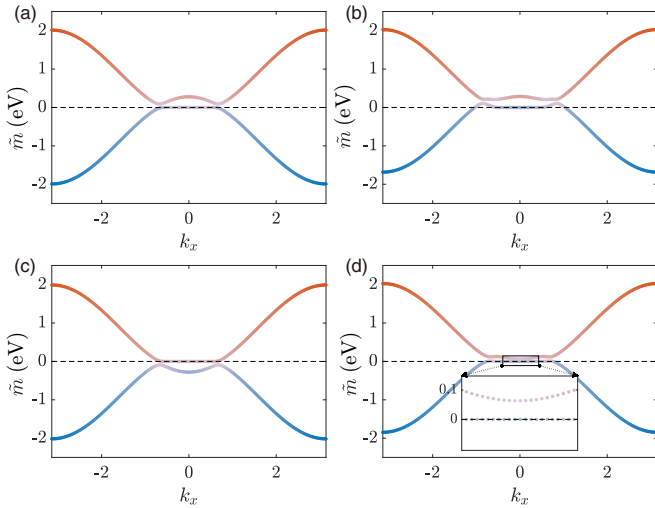


FIG. 3. Evolution of the effective mass $\tilde{m}_{n,\chi}(k_x, k_y = 0)$ ($n = 1, 2$), $\tilde{m}_{1,\chi}$ and $\tilde{m}_{2,\chi}$ (a) with $\chi = +$ at $\alpha = 0$, (b) with $\chi = +$ at $\alpha = 0.9$, (c) with $\chi = -$ at $\alpha = 0$, and (d) with $\chi = -$ at $\alpha = 0.9$.

coupling $H_{\parallel} = \sum_{l_z, \mathbf{k}} \Psi_{l_z, \mathbf{k}}^{\dagger} \lambda_{\parallel} (\sin k_x \sigma_x + \sin k_y \sigma_y) \tau_x \Psi_{l_z, \mathbf{k}}$. The part $H_{1D}(\alpha)$ for each \mathbf{k} is equivalent to a one-dimensional TI with the k -dependent band gap $m(\mathbf{k}) = m_0 - 4t_{\parallel} (\sin^2 \frac{k_x}{2} + \sin^2 \frac{k_y}{2})$ in a Zeeman field. In this case, $[\sigma_z, H_{1D}] = 0$, such that H_{1D} can be diagonalized to have a series of energy eigenvalues $\tilde{m}_{n,\chi}(k_x, k_y)$ and eigenvectors $\tilde{\Phi}_{k,n,\chi} = \sum_{l_z} U_{n,\chi;l_z} \Psi_{l_z, \mathbf{k}}$, with $n = 1, \dots, L_z$ and $\chi = \pm$. Using the eigenvectors as a new basis, we find that H_{tot} is equivalently reduced to a series of two-dimensional Dirac-like models $H_{\text{tot}} \equiv \sum_{\mathbf{k}, n, \chi = \pm 1} \tilde{\Phi}_{\mathbf{k}, n, \chi}^{\dagger} h_{n,\chi}(\mathbf{k}) \tilde{\Phi}_{\mathbf{k}, n, \chi}$, with

$$h_{n,\chi}(\mathbf{k}) = \lambda_{\parallel} (\sin k_x \sigma_x + \sin k_y \sigma_y) + \tilde{m}_{n,\chi}(\mathbf{k}, \alpha) \sigma_z. \quad (2)$$

The energy dispersions are $E_{n,\chi,\pm} = \pm \sqrt{\lambda_{\parallel}^2 (\sin^2 k_x + \sin^2 k_y) + \tilde{m}_{n,\chi}^2}$, where $\tilde{m}_{n,\chi}$ plays the role of a momentum-dependent mass term for the Dirac fermions.

In the absence of magnetic doping, i.e., $\alpha = 0$, H_{1D} can be solved exactly. For details, the solutions of the energy and wave function can be found in Ref. [36]. The masses have the relation $\tilde{m}_{n,+} = -\tilde{m}_{n,-} = m_n$, which gives rise to double degeneracy in the band structure rooted in the combination of the time-reversal symmetry and inversion symmetry. For $m(\mathbf{k}) > 0$, H_{1D} is topologically nontrivial and has zero-energy modes $m_1 = 0$; for $m(\mathbf{k}) < 0$, H_{1D} is topologically trivial, and the lowest-energy modes $m_1 = m(\mathbf{k})$. Here the film is thick enough that the finite-size effect can be ignored [38]. Therefore, in Eq. (2), $n = 1$ corresponds to the pair of gapless bands shown in Fig. 2. The spatial distribution of the wave function of $m_1 = 0$ is mainly concentrated near the top and bottom surfaces, as expected. The states with nonzero m_1 or at large k are spatially distributed in the bulk, which indicates that the surface states evolve into the bulk states with the variation of the wave vector \mathbf{k} . Here the complete band structure of the gapless Dirac fermions in the entire Brillouin zone consists of the surface fermions for $m(\mathbf{k}) > 0$ or small \mathbf{k} and those extended in the z direction for $m(\mathbf{k}) < 0$ or large \mathbf{k} [see Fig. 3(a)]. For $n \geq 2$, all $m_n(\mathbf{k})$ at $\mathbf{k} = 0$ are not equal to zero, which means the energy bands $E_{n,\chi}$

open an energy gap at the point (see Sec. SI in Ref. [36]). For a small \mathbf{k} , $h_{n,\chi}(\mathbf{k}) \simeq \lambda_{\parallel} (k_x \sigma_x + k_y \sigma_y) + \chi m_n(0) \sigma_z$. In other words, all the bands can be regarded as massive Dirac fermions.

In the presence of magnetic doping, the Zeeman field V_Z will change the band structures by altering effective mass \tilde{m} , while the linear part vertical to the z direction remains unchanged due to the degrees of freedom decoupling. In the basis of the energy eigenstates of $H_{1D}(\alpha)$ at $\alpha = 0$, the Zeeman term can be expressed as $\alpha \mathbf{I}_S(\mathbf{k}) \tau_0 \sigma_z$, where $\mathbf{I}_S(\mathbf{k})$ is an $L_z \times L_z$ matrix (see Sec. SII in Ref. [36]) that is numerically computable. Thus, H_{1D} is projected into the form $[\bigoplus_{n=1}^{L_z} m_n \tau_z + \alpha \mathbf{I}_S(\mathbf{k}) \tau_0 \sigma_z]$, and further diagonalizing this provides a bijection which maps the projected Hamiltonian form into the mass term $\bigoplus_n \tilde{m}_{n,\chi}(\mathbf{k}, \alpha) \sigma_z$. Confining ourselves to the subspace with $\sigma_z = +$, we can then track the evolution and interaction of the mass terms $\tilde{m}_{n,\chi}$ between $n = 1$ and $n = 2$ blocks with increasing α for a given χ . What stands out in the process is an exotic grafting behavior illustrated in Fig. 3: viewed from left to right, while the masses $\tilde{m}_{n,+}$ ($n = 1, 2$) maintain their shapes, $\tilde{m}_{n,-}$ ($n = 1, 2$), which represent one massless Dirac cone plus one massive Dirac cone, will fully exchange their low-energy parts with increasing α , i.e., massless \longleftrightarrow massive. By increasing α , $\tilde{m}_{n=1,-}$ and $\tilde{m}_{n=2,-}$ behave as if they cross around $\alpha_c \approx 0.74$ and then separate, during which the detailed dynamic exchange is revealed (see Sec. SV in Ref. [36]). On the other hand, what essentially remains unchanged is the high-energy part of each cone. Then since $\tilde{m}_{n,\chi}$, with $n = 1, 2$, are naturally assigned with opposite signs for their high-energy parts, viewed from the low-energy perspective, their high-energy masses exchange between massless and massive cones. The induced mass exchange of the massless and massive Dirac fermions is closely associated with the sign change of the Hall conductance.

Quantized Hall conductance. The Hamiltonian in Eq. (2) can be expressed in terms of the spin texture $\mathbf{d} = (\lambda_{\parallel} \sin k_x, \lambda_{\parallel} \sin k_y, \tilde{m}_{n,\chi}(k_x, k_y)) / E_{n,+}$, $h_{n,\chi} = E_{n,+} \mathbf{d} \cdot \boldsymbol{\sigma}$. Using the Kubo formula, the Hall conductance is given by

$$\sigma_H = -\frac{e^2}{h} \frac{1}{4\pi} \int \frac{dk_x dk_y}{4\pi} \mathbf{d} \cdot [\partial_{k_x} \mathbf{d} \times \partial_{k_y} \mathbf{d}] (f_{k,+} - f_{k,-}), \quad (3)$$

where $f_{k,\pm} = \Theta(\mu - E_{n,\pm})$ is the Heaviside step function for the Fermi-Dirac distribution at zero temperature and μ is the chemical potential [7,39]. For the massive Dirac fermions, the values of $\tilde{m}_{n,\chi}$ at $\mathbf{k} = (0, 0)$ and $\mathbf{k} = (\pi, \pi)$ have the same sign, and band inversion does not exist in the first Brillouin zone. The bands are always topologically trivial such that the fully filled bands, i.e., $\mu = 0$, always have no Hall conductance, which is consistent with the Thouless-Kohmoto-Nightingale-den Nijs theorem [10]. For massless Dirac fermions, $\tilde{m}_{n,\chi} = 0$ near $\mathbf{k} = 0$. In this regime, $\mathbf{d} \cdot [\partial_{k_x} \mathbf{d} \times \partial_{k_y} \mathbf{d}] = 0$, which indicates that the Berry curvature of the band vanishes. Nonzero Berry curvature comes only from the part of nonzero $\tilde{m}_{n,\chi}$ or the regime of large k . The Hall conductance is half quantized for μ located within the regime

of $\tilde{m}_{n,\chi} = 0$, $\sigma_H = \frac{e^2}{2h} \text{sgn}[\tilde{m}_{n,\chi}(\pi, \pi)]$. The quantization is protected by the emergent parity symmetry near the Fermi surface [29,40].

Based on the mass-exchange picture, we have a theoretical explanation for the change in the Hall conductance induced by the Zeeman field in Figs. 2(c) and 2(d). The film hosts a series of massive and massless Dirac fermions. For our purpose, we focus on the bands of $n = 1$ and $n = 2$ because all other massive Dirac fermions ($n \geq 3$) make no contribution to the Hall conductance when they are fully filled for a chemical potential near $\mu = 0$. In the absence of the Zeeman field, the film hosts a pair of massless Dirac fermions, in which one has $+\frac{e^2}{2h}$ and the other has $-\frac{e^2}{2h}$ due to the sign difference of the mass terms at large k . The total Hall conductance is zero, as expected. The presence of a weak Zeeman field does not change this situation. Nevertheless, with a holistic view, when the Zeeman field is increased further, one massless Dirac fermion and one massive Dirac fermion exchange their low-energy masses; meanwhile, their higher-energy parts remain unchanged but have different signs. Equivalently, the massless Dirac fermion changes the sign of the massive term at higher energy as viewed from the low-energy perspective. Consequently, its Hall conductance changes from $+\frac{e^2}{2h}$ to $-\frac{e^2}{2h}$. During this process, the other massless Dirac Fermion remains with its negative half-quantized Hall conductance unchanged, and the addition of two massless Dirac fermions gives a quantized Hall conductance of $-\frac{e^2}{2h} - \frac{e^2}{2h} = -\frac{e^2}{h}$.

Absence of chiral edge states. There are no chiral edge states around the system boundary in these paired gapless Dirac fermions. The quantum Hall conductance is not governed by the Chern number and does not satisfy the conventional bulk-edge correspondence [12]. We calculated the local density states at the x - z open surface at $y = 0$ with the wave vector k_x as a function of l_z in Fig. 4(a), where there is clearly no dispersion that connects the lateral surface valence and conduction bands, which is opposite to the conventional case. This illustrates explicitly that chiral edge states do not exist along the system boundary. The asymmetric local density of states between k_x and $-k_x$ reflects the fact that a chiral edge current exists for the filled bulk states. The states carrying the chiral edge current gradually become prominent when immersed in the middle of z from its top surface. Furthermore, it is found that a chiral edge current whose amplitude is proportional to the chemical potential still exists due to the time-reversal symmetry breaking caused by the Zeeman coupling [28]. As the Zeeman field is parallel to the lateral surface, the lateral surface states remain gapless. For comparison, we also present the local density of states for a magnetic sandwich heterostructure exhibiting the conventional or insulating QAHE in Fig. 4(b). The Hall conductance is $\sigma_H = -\frac{e^2}{h}$ and was measured experimentally [34,41]. It is shown that a linear dispersion connects the valence and conduction bands, evidencing the existence of a chiral edge state. This reflects the bulk-edge correspondence in the conventional QAHE. This is opposite to Fig. 4(a). The

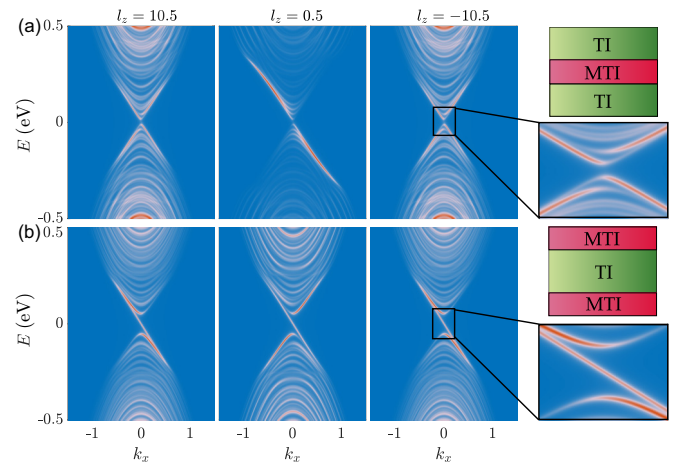


FIG. 4. The lateral local densities of states $\rho(l_z, k_x, E)$ for (a) metallic and (b) insulating/conventional QAHE in a magnetic topological insulator thin film. (a) The middle magnetic layer of $m_z = 6$. (b) The top and bottom magnetic layers of $m_z = 2$. The film thickness is $L_z = 22$, and the lattice site $l_z = \pm 1/2, \dots, \pm(L_z - 1)/2$. The width $L_y = 20$. Three equal-size plots shown from left to right indicate the local density of states at three different positions, $l_z = 10.5$ (top), $l_z = 0.5$ (middle), and $l_z = -10.5$ (bottom). The rightmost plots provide schematic side-view diagrams of the system, together with the amplified local density of states near $(k_y, E) \sim (0, 0)$ at the y -front bottom. The Zeeman field $\alpha = 0.8$.

presence and absence of the chiral edge states illustrate the topological distinction of the two phases, although their Hall conductances are identical.

Discussion. In the field theory, the massless Dirac fermions possess parity symmetry. When the Dirac fermions are coupled to the electromagnetic field, its action fails to restore the symmetry in any regularization and is characterized by a half-quantized Hall conductance. The discussion of the parity anomaly in condensed matter dates back to the early 1980s [42–44]. It has attracted extensive interest since the discovery of TIs, as the massless Dirac fermions can exist on the surface [45–47]. The film here provides a platform to explore the related physics of the parity anomaly. The massless Dirac fermions on the surfaces are accompanied by the presence of the nonzero zero term $\tilde{m}_{n,\chi}$ at large k , which plays the role of the regulator of Dirac fermions in the field theory. Thus, the nonzero Hall conductance is determined by just the sign of $\tilde{m}_{n,\chi}$ at $k = 0$ and large k , independent of the specific form and the amplitude of $\tilde{m}_{n,\chi}$. In this sense, the present work reflects the physics of the quantum anomaly. However, we should keep in mind that the term has already broken the parity symmetry explicitly.

Acknowledgment. This work was supported by the Research Grants Council, University Grants Committee, Hong Kong under Grants No. C7012-21G and No. 17301823 and the National Key R&D Program of China under Grant No. 2019YFA0308603.

- [1] F. D. M. Haldane, *Phys. Rev. Lett.* **61**, 2015 (1988).
- [2] R. Yu, W. Zhang, H.-J. Zhang, S.-C. Zhang, X. Dai, and Z. Fang, *Science* **329**, 61 (2010).
- [3] Z. Qiao, S. A. Yang, W. Feng, W.-K. Tse, J. Ding, Y. Yao, J. Wang, and Q. Niu, *Phys. Rev. B* **82**, 161414(R) (2010).
- [4] R.-L. Chu, J. Shi, and S.-Q. Shen, *Phys. Rev. B* **84**, 085312 (2011).
- [5] C.-X. Liu, S.-C. Zhang, and X.-L. Qi, *Annu. Rev. Condens. Matter Phys.* **7**, 301 (2016).
- [6] C.-Z. Chang, C.-X. Liu, and A. H. MacDonald, *Rev. Mod. Phys.* **95**, 011002 (2023).
- [7] S.-Q. Shen, *Topological Insulators*, 2nd ed., Springer Series in Solid State Science Vol. 187 (Springer, Singapore, 2017).
- [8] B. I. Halperin, *Phys. Rev. B* **25**, 2185 (1982).
- [9] B. I. Halperin, *Rev. Mod. Phys.* **92**, 045001 (2020).
- [10] D. J. Thouless, M. Kohmoto, M. P. Nightingale, and M. den Nijs, *Phys. Rev. Lett.* **49**, 405 (1982).
- [11] Q. Niu, D. J. Thouless, and Y.-S. Wu, *Phys. Rev. B* **31**, 3372 (1985).
- [12] Y. Hatsugai, *Phys. Rev. Lett.* **71**, 3697 (1993).
- [13] C.-Z. Chang *et al.*, *Science* **340**, 167 (2013).
- [14] C.-Z. Chang, W. Zhao, D. Y. Kim, H. Zhang, B. A. Assaf, D. Heiman, S.-C. Zhang, C. Liu, M. H. Chan, and J. S. Moodera, *Nat. Mater.* **14**, 473 (2015).
- [15] J. Checkelsky, R. Yoshimi, A. Tsukazaki, K. Takahashi, Y. Kozuka, J. Falson, M. Kawasaki, and Y. Tokura, *Nat. Phys.* **10**, 731 (2014).
- [16] X. Kou, S.-T. Guo, Y. Fan, L. Pan, M. Lang, Y. Jiang, Q. Shao, T. Nie, K. Murata, J. Tang, Y. Wang, L. He, T.-K. Lee, W.-L. Lee, and K. L. Wang, *Phys. Rev. Lett.* **113**, 137201 (2014).
- [17] Y. Okazaki, T. Oe, M. Kawamura, R. Yoshimi, S. Nakamura, S. Takada, M. Mogi, K. S. Takahashi, A. Tsukazaki, M. Kawasaki, Y. Tokura, and N.-H. Kaneko, *Nat. Phys.* **18**, 25 (2022).
- [18] J. Li, Y. Li, S. Du, Z. Wang, B.-L. Gu, S.-C. Zhang, K. He, W. Duan, and Y. Xu, *Sci. Adv.* **5**, eaaw5685 (2019).
- [19] Y. Deng, Y. Yu, M. Z. Shi, Z. Guo, Z. Xu, J. Wang, X. H. Chen, and Y. Zhang, *Science* **367**, 895 (2020).
- [20] M. M. Otrokov *et al.*, *Nature (London)* **576**, 416 (2019).
- [21] C. Liu, Y. Wang, H. Li, Y. Wu, Y. Li, J. Li, K. He, Y. Xu, J. Zhang, and Y. Wang, *Nat. Mater.* **19**, 522 (2020).
- [22] Y. Gong *et al.*, *Chin. Phys. Lett.* **36**, 076801 (2019).
- [23] Y. J. Chen, L. X. Xu, J. H. Li, Y. W. Li, H. Y. Wang, C. F. Zhang, H. Li, Y. Wu, A. J. Liang, C. Chen, S. W. Jung, C. Cacho, Y. H. Mao, S. Liu, M. X. Wang, Y. F. Guo, Y. Xu, Z. K. Liu, L. X. Yang, and Y. L. Chen, *Phys. Rev. X* **9**, 041040 (2019).
- [24] B. Chen *et al.*, *Nat. Commun.* **10**, 4469 (2019).
- [25] M. Liu, W. Wang, A. R. Richardella, A. Kandala, J. Li, A. Yazdani, N. Samarth, and N. P. Ong, *Sci. Adv.* **2**, e1600167 (2016).
- [26] K. Yasuda, M. Mogi, R. Yoshimi, A. Tsukazaki, K. Takahashi, M. Kawasaki, F. Kagawa, and Y. Tokura, *Science* **358**, 1311 (2017).
- [27] M. Mogi, Y. Okamura, M. Kawamura, R. Yoshimi, K. Yasuda, A. Tsukazaki, K. Takahashi, T. Morimoto, N. Nagaosa, M. Kawasaki, Y. Takahashi, and Y. Tokura, *Nat. Phys.* **18**, 390 (2022).
- [28] J.-Y. Zou, B. Fu, H.-W. Wang, Z.-A. Hu, and S.-Q. Shen, *Phys. Rev. B* **105**, L201106 (2022).
- [29] J.-Y. Zou, R. Chen, B. Fu, H.-W. Wang, Z.-A. Hu, and S.-Q. Shen, *Phys. Rev. B* **107**, 125153 (2023).
- [30] Y. Tokura, K. Yasuda, and A. Tsukazaki, *Nat. Rev. Phys.* **1**, 126 (2019).
- [31] H. Zhang, C.-X. Liu, X.-L. Qi, X. Dai, Z. Fang, and S.-C. Zhang, *Nat. Phys.* **5**, 438 (2009).
- [32] Y. Chen, J.-H. Chu, Z. Liu, S.-K. Mo, H. Zhang, D. Lu, X. Dai, Z. Fang, S.-C. Zhang, I. Fisher, Z. Hussain, and Z.-X. Shen, *Science* **325**, 178 (2009).
- [33] Y. Zhang, K. He, C.-Z. Chang, C.-L. Song, L.-L. Wang, X. Chen, J.-F. Jia, Z. Fang, X. Dai, W.-Y. Shan, S. Q. Shen, Q. Niu, X. L. Qi, S. C. Zhang, X. C. Ma, and Q. K. Xue, *Nat. Phys.* **6**, 584 (2010).
- [34] Y.-F. Zhao, R. Zhang, R. Mei, L.-J. Zhou, H. Yi, Y.-Q. Zhang, J. Yu, R. Xiao, K. Wang, N. Samarth, M. H. W. Chan, C. X. Liu, and C. Z. Chang, *Nature (London)* **588**, 419 (2020).
- [35] C.-X. Liu, X.-L. Qi, H. J. Zhang, X. Dai, Z. Fang, and S.-C. Zhang, *Phys. Rev. B* **82**, 045122 (2010).
- [36] See Supplemental Material at <http://link.aps.org/supplemental/10.1103/PhysRevB.108.L241407> for details of the derivation of Eq. (2) at $\alpha = 0$ (Sec. SI), the Zeeman term (Sec. SII), a case study of the conventional anomalous Hall effect (Sec. SIII), a case study of $\alpha = 0.9$ explained by only $n - 1, 2$ (Sec. SIV), the fine process near the transition (Sec. SV), and the local density of the chiral current (Sec. SVI), which includes Refs. [28,48].
- [37] G. Mahan, *Many-Particle Physics* (Plenum, New York, 1981).
- [38] H.-Z. Lu, W.-Y. Shan, W. Yao, Q. Niu, and S.-Q. Shen, *Phys. Rev. B* **81**, 115407 (2010).
- [39] X.-L. Qi, T. L. Hughes, and S.-C. Zhang, *Phys. Rev. B* **78**, 195424 (2008).
- [40] B. Fu, J.-Y. Zou, Z.-A. Hu, H.-W. Wang, and S.-Q. Shen, *npj Quantum Mater.* **7**, 94 (2022).
- [41] M. Mogi, R. Yoshimi, A. Tsukazaki, K. Yasuda, Y. Kozuka, K. Takahashi, M. Kawasaki, and Y. Tokura, *Appl. Phys. Lett.* **107**, 182401 (2015).
- [42] A. J. Niemi and G. W. Semenoff, *Phys. Rev. Lett.* **51**, 2077 (1983).
- [43] A. N. Redlich, *Phys. Rev. Lett.* **52**, 18 (1984).
- [44] E. Fradkin, E. Dagotto, and D. Boyanovsky, *Phys. Rev. Lett.* **57**, 2967 (1986).
- [45] S. Zhang, L. Pi, R. Wang, G. Yu, X.-C. Pan, Z. Wei, J. Zhang, C. Xi, Z. Bai, F. Fei, M. Wang, J. Liao, Y. Li, X. Wang, F. Song, Y. Zhang, B. Wang, D. Xing, and G. Wang, *Nat. Commun.* **8**, 977 (2017).
- [46] J. Böttcher, C. Tutschku, L. W. Molenkamp, and E. M. Hankiewicz, *Phys. Rev. Lett.* **123**, 226602 (2019).
- [47] H.-W. Wang, B. Fu, and S.-Q. Shen, *Phys. Rev. B* **104**, L241111 (2021).
- [48] J. Krimmer, QUIVER, magnitude-dependent color in 2D and 3D, MATLAB Central File Exchange, 2023, <https://ww2.mathworks.cn/matlabcentral/fileexchange/58527-quivermagnitudedependent-color-in-2d-and-3d>.